Journal of Magnetics 15(2), 56-60 (2010) DOI: 10.4283/JMAG.2010.15.2.056

Composition-dependent Magnetic Properties of $Si_{1-x}Mn_x$ ($0.1 < x < 0.9$) Single Crystals

Younghun Hwang[1], Youngho Um[1], and Hyo-yeol Park[2]*

[1]*Department of Physics, University of Ulsan, Ulsan 680-749, Korea*
[2]*Semiconductors Applications, Ulsan College, Ulsan 680-749, Korea*

(Received 27 May 2010, Received in final form 17 June 2010, Accepted 18 June 2010)

In this study, we investigated the optical, magnetic, and electrical transport properties of $Si_{1-x}Mn_x$ ($0.1 < x < 0.9$) single crystals grown by the vertical Bridgman method. The alloys with a Mn concentration of up to 64% demonstrated weak ferromagnetic ordering around $T_C = 30$ K. The $Si_{0.25}Mn_{0.75}$ and $Si_{0.18}Mn_{0.82}$ alloys showed weak ferromagnetic ordering at 70 K and antiferromagnetic ordering at 104 K, as confirmed by magnetization, neutron diffraction, and transport studies.

Keywords : SiMn, magnetic transition, weak ferromagnetic

1. Introduction

Cubic transition metal silicies *M*Si (*M*=Cr, Mn, Fe, Co) with a B20 structure have attracted the attention of a number of investigators because of their varied magnetic and transport properties [1-3]. For example, CrSi demonstrates paramagnetic (PM) behavior with essentially temperature-independent susceptibility [1], FeSi exhibits unusual temperature-independent paramagnetic behavior [3], and CoSi is diamagnetic with temperature-independent susceptibility [4]. Weak ferromagnetism appears in the solid solution between FeSi and CoSi [5]. MnSi in a zero magnetic field has a helical spin structure with a long period (180 Å) in the ordered state below a T_C of about 29 K [6, 7]. The helical spin state was observed to change into an induced ferromagnetic (FM) spin state by external magnetic fields. The induced ferromagnetic moment of 0.4 μ_B per Mn at 6.2 kOe is much smaller than the effective magnetic moment of 1.4 μ_B per Mn determined from the Curie constant in the paramagnetic region [8, 9]. Currently, little is known about Mn composition-dependent magnetic and transport properties. In this work, we investigated the magnetic and electrical transport properties of $Si_{1-x}Mn_x$ single crystals. The alloys with a Mn concentration up to 64% demonstrated weak ferromagnetic ordering around a T_C of ~30 K, while $Si_{0.25}Mn_{0.75}$ and $Si_{0.18}Mn_{0.82}$ alloys showed weak ferromagnetic ordering at 70 K and antiferromagnetic (AFM) ordering at 104 K, as confirmed by magnetization, electrical transport, and neutron diffraction studies.

*Corresponding author: Tel: +82-52-279-3282
Fax: +82-52-279-3182, e-mail: hypark@uc.ac.kr

2. Experiment

The $Si_{1-x}Mn_x$ single crystals were grown in a double furnace using the vertical Bridgman method with Si(6N) and Mn(4N) elements. The elements were put into an ampoule which had a capillary bottom in order to grow only one seed after the inside wall of the quartz ampoule was coated with carbon. Then, the ampoule was evacuated and sealed under a pressure of ~10^{-6} Torr and placed in the furnace. The upper and lower furnaces were maintained at 1,260°C and 760°C, respectively. The ampoule was held at 1,260°C for 5 hours, and its position was lowered slowly at a rate of 1.4 mm/hr. The solidification gradient in the furnace was 22.5°C/cm. The obtained crystal had a cylindrical form with a diameter of 10 mm and a length of 20 mm. The composition and homogeneity of the grown single crystals were evaluated by an electron probe microanalyzer (EPMA-1400, SHIMADZU), inductively coupled plasma (ICP-Atomscan25, Thermo Jarrell Ash), and energy dispersion spectra (EDS, FE-SEMJSM6500F, Japan). Laue and X-ray diffraction (XRD) studies were performed in order to characterize the $Si_{1-x}Mn_x$ crystal structure. For the structural and magnetic analysis, neutron diffraction was conducted using a high-resolution powder diffractometer (HRPD of HANARO at the Korea Atomic Energy Research Institute) with a Ge

(331) monochromator and a neutron wavelength of λ = 1.834 Å, while a closed-cycle refrigerator (CCR) was used to control the temperature from 10 to 300 K.

3. Results and Discussion

Fig. 1 shows the experimental (a, b, and c) and simulated (d, e, and f) Laue patterns for $Si_{1-x}Mn_x$ with x=0.17 (a and d), 0.49 (b and e), and 0.75 (c and f), illustrating the SiMn single crystal. The temperature θ-2θ XRD spectra for powdered $Si_{1-x}Mn_x$ single crystals are shown in Fig. 2(a). The observed XRD patterns for all crystals were found to be a cubic structure. The lattice constants increased with Mn concentration up to 82%, as shown in Fig. 2(b), and followed the fitted linear relationship of 4.480+0.149x (Å) ($0.1 < x < 0.9$), due to the larger Mn atomic radius (1.40 Å), as compared to Si (1.10 Å). The increase in the lattice constant with increasing Mn concentration shows that Mn ions are substitutionally incorporated into the host Si sites up to x = 82%. The mole fractions obtained by ICP, EPMA, and EDS methods are shown in Fig. 2(c). The results obtained from these three methods were similar for all compositions, and the average values of the three results were used as the Mn mole fractions.

The optical absorption measurements were performed at room temperature with a UV VIS-NIR U-3501 (Hitachi) spectrophotometer in the spectral range of 0.47 to 6.2 eV. The absorption coefficients (α) for the $Si_{1-x}Mn_x$ crystal were calculated from the absorption spectra. The absorption coefficient was governed by the formula for allowed direct transition, $(\alpha \cdot h\nu)^2 \sim (h\nu \sim E_g)$, as the direct transition in this system was confirmed from the plot of $(\alpha \cdot h\nu)^2$ vs $h\nu$ for various Mn compositions at 300 K. The values of the corresponding band gap energy (E_g) were estimated by extrapolation of the apparent linear region, revealing the existence of the direct band gap. In addition, the band gap measured by the absorption spectra at room

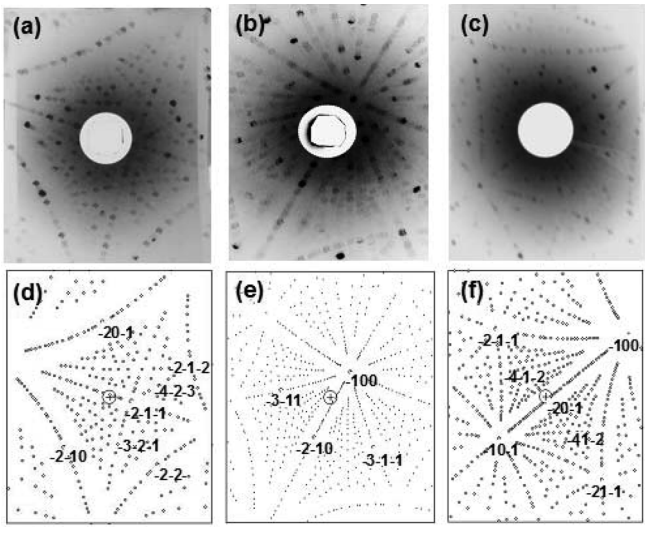

Fig. 1. The experimental (a, b, c) and simulated (d, e, f) Laue patterns for $Si_{1-x}Mn_x$ with x = 0.17 (a, d), 0.49 (b, e), and 0.75 (c, f), illustrating the single crystal SiMn.

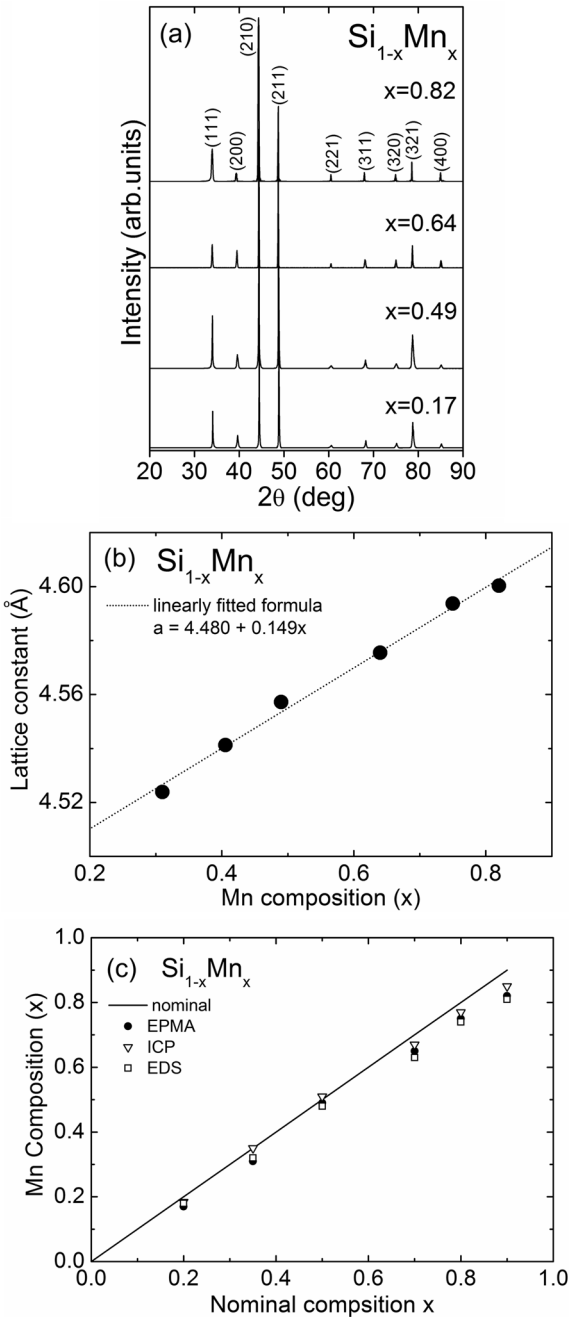

Fig. 2. (a) θ-2θ XRD spectra of the powdered $Si_{1-x}Mn_x$ crystals. (b) Lattice constants as a function of the Mn composition (x). (c) The mole fractions of the $Si_{1-x}Mn_x$ single crystals determined using ICP, EPMA, and EDS methods.

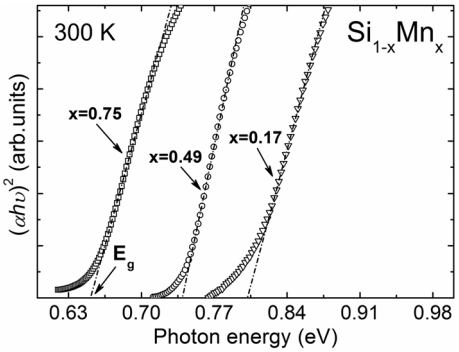

Fig. 3. Plots of $(\alpha \cdot h\nu)^2$ vs. the photon energy for $Si_{1-x}Mn_x$ crystals at 300 K. The extrapolated straight line from the straight portion was used to determine the value of E_g.

temperature decreased with the addition of Mn into Si, as shown in Fig. 3.

The optical band gaps of $Si_{1-x}Mn_x$ for x=0.17, 0.31, 0.49, 0.75, and 0.82 were measured to be 0.80, 0.77, 0.74, 0.65, and 0.62 eV, respectively. Note that previously reported energy gaps of $Si_{0.58}Mn_{0.42}$ are in the range of 0.68-0.83 eV [10-12]. The decrease of the energy gap with increasing Mn content may be due to an increase in the lattice constant.

The magnetic and transport properties were studied using a magnetic property measurement system (MPMS, Quantum Design, Inc.) and a physical property measurement system (PPMS, Quantum Design, Inc.), respectively.

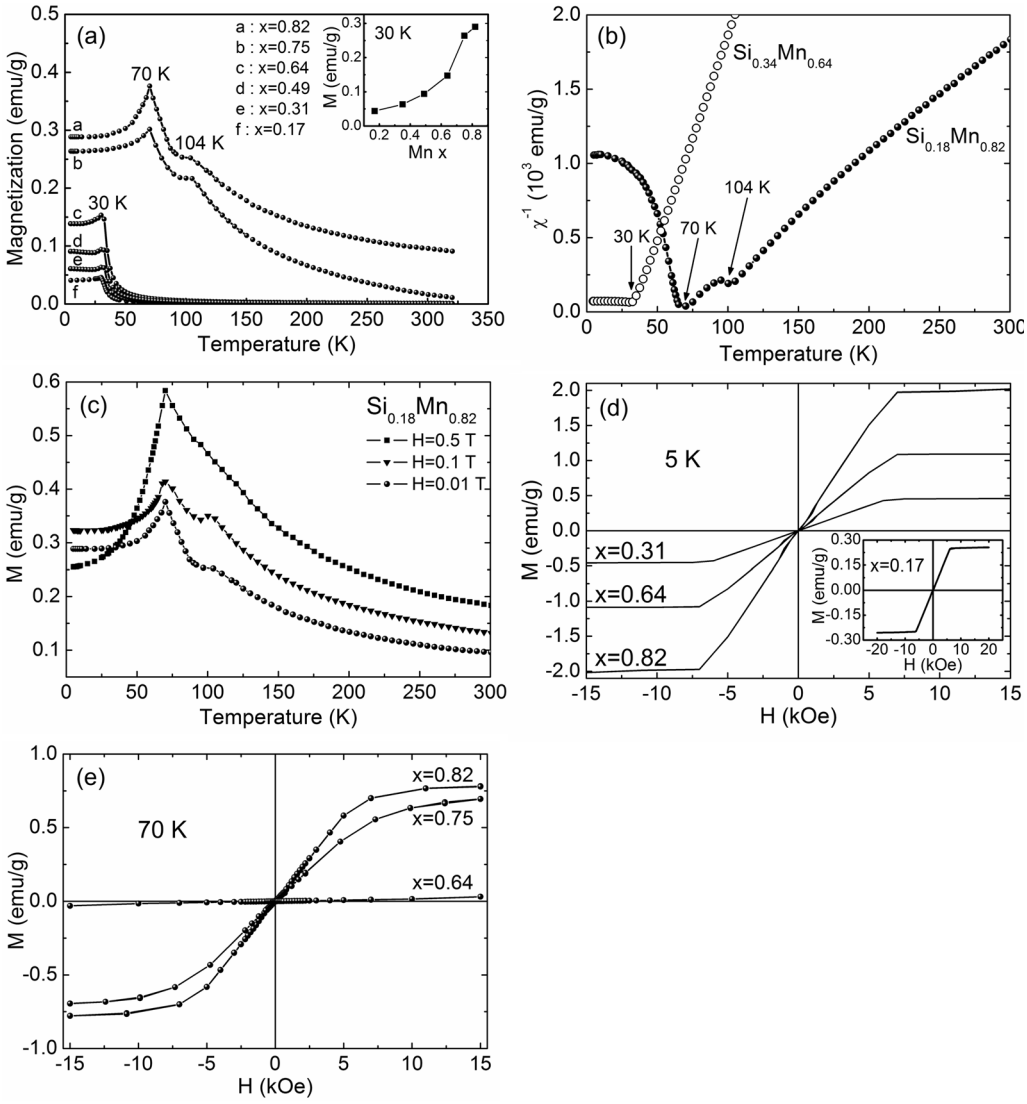

Fig. 4. (a) Temperature-dependent magnetization (M) of $Si_{1-x}Mn_x$ single crystals with x = 0.17, 0.31, 0.49, 0.64, 0.75, and 0.82 under an applied magnetic field of 100 Oe. The inset shows that the magnetization of $Si_{1-x}Mn_x$ at 30 K increases with increasing Mn concentration. (b) The reciprocal susceptibility, χ^{-1}, vs. T for $Si_{1-x}Mn_x$ crystals with x = 0.64 and 0.82. (c) The magnetic field-dependent M-T curves for x = 0.82 with H = 0.01, 0.1, and 0.5 T. The M-H loops showing hysteric behavior for the $Si_{1-x}Mn_x$ crystals with x = 0.17, 0.31, 0.49, 0.64, 0.75, and 0.82 at 5 K (d), and x = 0.75 and 0.82 at 70 K (e).

Fig. 4(a) shows the temperature (T) dependent magnetization (M) of $Si_{1-x}Mn_x$ single crystals with x=0.17, 0.31, 0.49, 0.64, 0.75, and 0.82 between 5 and 320 K with an applied magnetic field of 100 Oe. The magnetization increased with increasing Mn composition, as shown in the inset of Fig. 4(a). This result indicates that the spin-spin interactions should become enhanced by the addition of Mn. The magnetization of the crystals with $0.1 < x < 0.7$ shows a transition at 30 K and decreases rapidly with increasing temperature. The obtained transition temperature of 30 K agrees well with the previous result for MnSi [6,7]. However, for x=0.75 and 0.82, the data show two distinct transitions at 70 K and 104 K.

Fig. 4(b) shows the reciprocal of the susceptibility, χ^{-1}, vs. T for the $Si_{1-x}Mn_x$ crystals with x=0.64 and 0.82. From the Curie-Weiss law fitting of the inverse susceptibility, it was confirmed that the transition temperature at 70 K is the Curie point (T_C) for a ferromagnetic state. The magnetic field dependent M-T curves for x=0.82 are shown in Fig. 4(c). Transition points around 70 and 104 K are observed under low magnetic fields of 0.01 and 0.1 T. However, for $H > 0.1$ T, the cusp near 104 K disappeared. Therefore, the shape of the second transition curve (104 K) looks like a Neel temperature (T_N) [13].

In Fig. 4(d) and (e), the magnetization loops show hysteric behavior, indicating that the $Si_{1-x}Mn_x$ single crystal is ferromagnetic between 5 K and 70 K. The average magnetic moments per Mn at 5 K determined from the saturated magnetizations are 0.05, 0.10, 0.18, 0.21, 0.33, and 0.40 μ_B for x=0.17, 0.31, 0.49, 0.64, 0.75, and 0.82, respectively. Note that the magnetic moment per Mn (0.18 μ_B) for x=0.49 is lower than the previously reported value of 0.4 μ_B [8]. If we consider the Mn-spin, the average magnetic moment of transition metal impurities is expected to be much lower. These results indicate that the samples formed a secondary phase. However, it is remarkable that, with the Mn addition, the magnetic moment increased.

Fig. 5 shows the temperature dependence of the neutron diffraction of $Si_{0.18}Mn_{0.82}$. The magnetic peak intensity decreased with increasing temperature. The intensities of the magnetic peaks decreased with increasing temperature and disappeared above 70 K. This result shows that the phase transition occurs around 70 K, which is in good agreement with our magnetization data. We also investigated the transport properties of the samples. The carrier type (sign) and concentration were determined from Hall measurements. The samples with $0.17 \le x \le 0.64$ showed n-type conduction, while samples with $0.75 \le x \le 0.82$ demonstrated p-type conductivity at 300 K, as determined using the relation $n_H = -1/(eR_H)$. The effective carrier densities at 300 K were 8.78×10^{17}, 1.97×10^{18}, 5.15×10^{18}, 8.48×10^{18}, 6.56×10^{19}, and 5.78×10^{19} cm^{-3} for x = 0.17, 0.31, 0.49, 0.64, 0.75, and 0.82, respectively. For an alloy ratio, x, larger than 0.64, metallic transport in the formed impurity band is possible.

We measured the temperature dependence of the electrical resistivity (ρ) for x = 0.17, 0.31, 0.64, and 0.82, as shown in Fig. 6. For $x < 0.7$, a slope change in the resistivity is observed at 30 K, corresponding to a ferromagnetic-paramagnetic phase transition, which is in good agreement with the magnetization data. For $x > 0.7$, the resistivity increased monotonically for temperatures up to 70 K and then decreased up to 104 K before increasing again. The two distinct slope changes at about 70 and 104 K correspond to the FM-AFM and AFM-PM transition temperatures in the M-T measurements, respectively. These resistivity changes at the phase transitions are presumably due to changes in the spin-flip scattering rates at the FM-AFM and AFM-PM transitions. Compared to

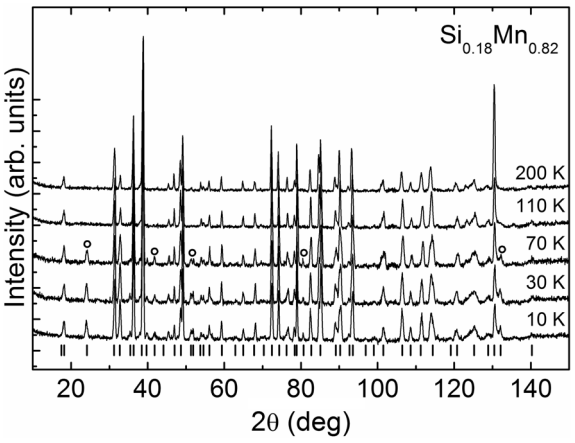

Fig. 5. Temperature dependence of the neutron diffraction for the $Si_{0.18}Mn_{0.82}$ crystal. The open circle denotes the peaks with the magnetic contribution.

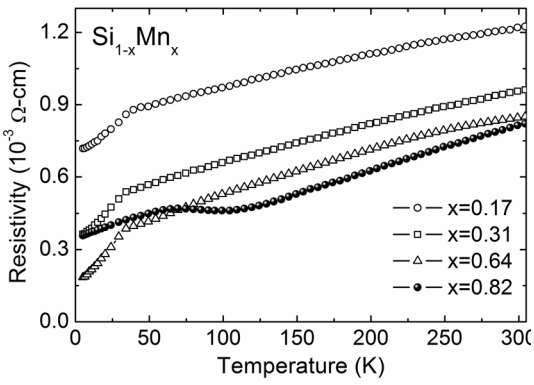

Fig. 6. Temperature dependence of the resistivity of the $Si_{1-x}Mn_x$ crystals.

the magnetization measurements, which can also include local effects, such as magnetic impurity clusters, resistivity data provides an alternate technique to study the transition, which is averaged over the entire sample. Thus, the temperature dependent resistivity results strongly support the presence of phase transitions (FM-AFM and AFM-PM) at 70 and 104 K, respectively.

4. Conclusion

We investigated the magnetic and transport properties of $Si_{1-x}Mn_x$ single crystals by applying the vertical Bridgman method. The $Si_{1-x}Mn_x$ single crystals were ferromagnetic up to 70 K. The average magnetic moment was 0.40 μ_B/Mn at 5 K for the $Si_{0.18}Mn_{0.82}$ crystal. Even though the measured magnetic moment per Mn atom at 0.7 T was very low for $Si_{1-x}Mn_x$ with a high value of x, the magnetic moment increased with Mn addition. The transport properties of $Si_{1-x}Mn_x$ with a large value of x were found to be similar to the magnetic properties.

Acknowledgments

This work was supported by Priority Research Centers Program through the National Research Foundation of Korea (NRF), funded by the Ministry of Education, Science, and Technology (2009-0093818).

References

[1] H. J. Williams, J. H. Wernick, R. C. Sherwood, and G. K. Wertheim, J. Appl. Phys. **37**, 1256 (1966).
[2] D. Shinoda and S. Asanabe, J. Phys. Soc. Jpn. **21**, 555 (1966).
[3] V. Jaccarino, G. K. Wertheim, J. H. Wernick, L. R. Walker, and S. Arajs, Phys. Rev. **160**, 476 (1967).
[4] G. K. Wertheim, J. H. Wernick, and D. N. E. Buchanan, J. Appl. Phys. **37**, 3333 (1966).
[5] J. H. Wernick, G. K. Wertheim, and R. C. Sherwood, Mater. Res. Bull. **7**, 1431 (1971).
[6] Y. Ishikawa, K. Tajima, D. Bloch, and M. Roth, Solid State Commun. **19**, 525 (1976).
[7] Y. Ishikawa, G. Shirane, J. A. Tarvin, and M. Kohgi, Phys. Rev. B **16**, 4956 (1977).
[8] D. Bloch, J. Voiron, V. Jaccarino, and J. H. Wernick, Phys. Lett. A**51**, 259 (1975).
[9] L. M. Levinson, G. H. Lander, and M. O. Steinitz, AIP Conf. Proc. **10**, 1138 (1972).
[10] M. C. Bost and J. E. Mahan, J. Electron. Mater. **16**, 389 (1987).
[11] L. Zhang and D. G. Ivey, J. Mater. Sci. **2**, 116 (1991).
[12] S. Teichert, R. Kilper, J. Erben, D. Franke, B. Gebhard, Th. Franke, P. Häussler, W. Henrion, and H. Lange, Appl. Surf. Sci. **104-105**, 679 (1996).
[13] Y. H. Hwang, S. Cho, H. K. Kim, and Y. H. Um, J. Magn. Magn. Mater. **304**, e173 (2006).